A FULLY AUTOMATIC STRUCTURAL OPTIMIZATION FRAMEWORK TO DETERMINE CRITICAL DESIGN LOADS

Martin Leitner[1], René Liepelt[2], Thiemo M. Kier[1], Thomas Klimmek[2], Reiko Müller[1], Matthias Schulze[2]

[1]DLR, Institute of System Dynamics und Control
[2]DLR, Institute of Aeroelasticity

Abstract

Critical loads play an essential role in early aircraft design studies. In order to determine a consistent envelope of critical design loads, a framework has to be introduced in which the dynamic models for loads calculation and the static models for aircraft structural design have to be evaluated and analyzed in an iterative manner. In the course of the DLR project Digital-X a process was established that generically builds an initial aircraft structural model and sizes it in a global optimization loop using updated dynamic models for calculating the trim, gust and maneuver loads necessary to ensure structural integrity as prescribed by the Federal Aviation Regulations (FAR). In this paper the fully automated aeroelastic analysis, flight loads prediction and structural sizing process is presented that determines the design loads used in the Digital-X multidisciplinary design optimization (MDO) framework.

1. INTRODUCTION

Multidisciplinary integration in collaborative design activities is one of the main efforts of future developments towards highly efficient aircraft. Due to the continuing drive towards more lightweight aircraft designs, lifting surface deflections under load have become larger. This leads to an always growing importance of the integral discipline of loads calculation that strongly interfaces with the aerodynamic, structural and control design departments. Quasi-static and transient dynamic loads due to closed-loop and open-loop flight maneuvers and turbulence depend on the aerodynamic shape and flexibility of the aircraft and set the boundary conditions for structural design. To increase the accuracy in the early aircraft design stages, the use of integrated flight dynamic models that determine reliable loads is of great importance. The foundation of these models is usually given by a representative finite element model with realistic stiffness and mass properties that allows for various design modifications.

This paper presents the fully automated aeroelastic analysis and loads calculation process used in the Digital-X multidisciplinary design framework. The parametric structural modeling process MONA [1] is combined with the maneuver simulation tool Varloads ([2], [3]) to determine design loads of the XRF1 long range aircraft configuration. The MONA process combines the model generator ModGen [4] and the capabilities of MSC Nastran [5] for structural, aeroelastic, loads analysis and optimization. Within MONA the finite element model (FEM), the aerodynamic model, the aero-structure coupling model and the mass models are established. These are necessary to enable the linear, frequency domain aeroelastic and manoeuver trim analyses in NASTRAN. It also sets up the optimization model for structural sizing. Varloads uses the statically residualized structural and mass matrices along with the aerodynamic panel model to drive open or closed-loop, non-linear time-domain flight dynamics models for maneuver loads and gust analysis.

The loads and sizing process is integrated in the Digital-X multidisciplinary design analysis and optimization process chain depicted in Figure 1, where it is marked in red as the dynamic level. The MDO process is basically divided into three steps: preliminary design, loads calculation and the detailed analysis level. It includes aerodynamics, mass estimation, engine, flight performance and other disciplinary tools. It is a collaborative process chain assembled by several DLR institutes contributing their expertise [6]. The parameters necessary to run the MDO process are stored in a file using a common language developed by DLR [7]. The CPACS (Common Parametric Aircraft Configuration Schema) is a XML data format for parametric aircraft descriptions that uses auxiliary tools for data processing. The coupling and interaction of the analysis components is accomplished with the help of RCE (Remote Component Environment) [8]. The loads process extracts the necessary data from the CPACS input file, which includes geometry, secondary masses and operational characteristics of an aircraft. It returns the estimated wing mass and the nodal and cut loads of all lifting surfaces and the fuselage to

CPACS.

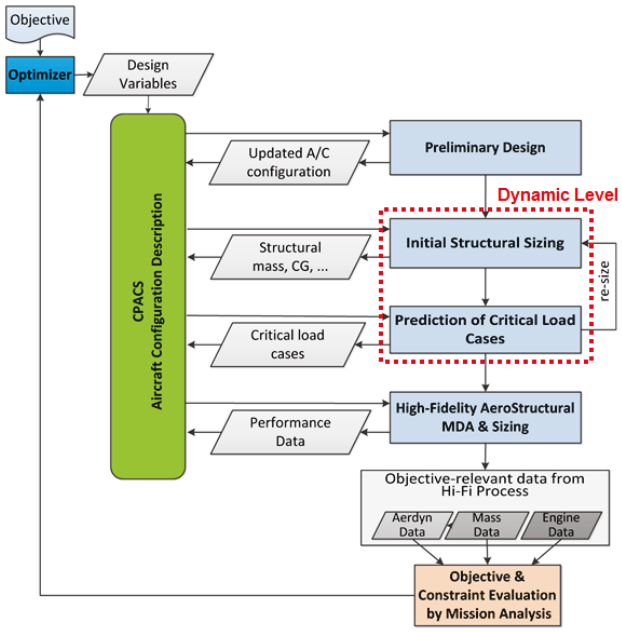

Figure 1. The Digital-X MDO process.

2. SIZING PROCESS

The general workflow of the main loads calculation process is depicted in Figure 2 and starts with reading the relevant geometric aircraft design parameters, following the latest CPACS conventions to correctly interpret the data. This information is used to build the underlying structural finite element, the aerodynamic panel and the coupling model from which the stiffness, the aerodynamic coefficient and the splining matrix can be solved. The aircraft global design mass data, as well as secondary masses, are calculated by tools in the preliminary design stage and are stored in the CPACS file as well. Multiple aircraft mass model configurations are set up, resulting from combinations of different fuel and payload conditions.

The initial stiffness of the structure and the distributed fuel mass cases are calculated in an afore-going, fast conceptual design phase, based on a rigid aircraft description [9]. Then the iterative loads calculation process is triggered, where the structural, aerodynamic and inertia coefficients are solved and reduced to lower the number of degrees of freedom (DoF), leading to lower memory consumption and calculation times.

After establishing the four building blocks of the aeroservoelastic tetrahedron - stiffness, mass, aerodynamics and control - the integrated frequency and time domain models are generated that are later on solved while complying with the boundary conditions of the optimization problem. Finally the load case specifications are read and executed. They mostly depend on the aircraft's flight envelope and operational properties and are based on the Federal Aviation Regulations [10] that set the airworthiness standards for transportation category airplanes. They include maneuver trim cases such as pull-up and dive maneuvers that are calculated with frequency domain equations of motion as well as gust and open-loop and close-loop maneuvers that are simulated in time domain. The loads are recovered using the rigid body and flexible states along with the structural, mass and aerodynamic coefficients following the Force Summation Method (FSM) [11]. The loads are then sorted and filtered to build the loads envelope relevant for sizing the aircraft's structural components. These critical loads are then reintroduced into the full FEM structure to drive inertia relieved static solutions to obtain the stress and strain distributions under load. Along with the boundary condition solution cases such as buckling, divergence and flutter the optimizer is able to determine the minimum component masses within the allowed spar, rib and skin thickness margins. The resulting structural dimensions and the component masses are temporarily stored in files that serve as input for the next iteration. Convergence is determined on the basis of absolute and relative change of the wing mass.

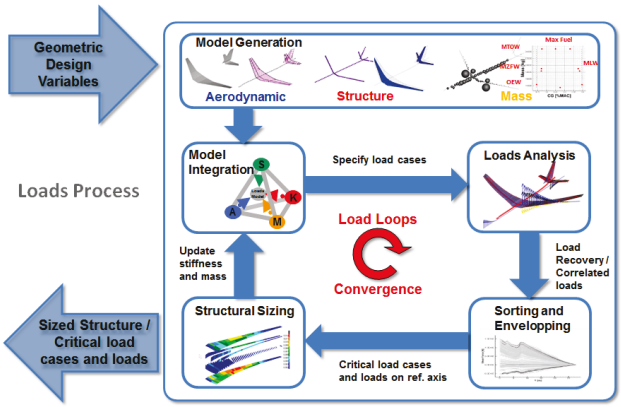

Figure 2. The generalized loads and sizing process.

3. MODEL GENERATION

3.1. Structural Models

The structural models are built with the help of the parametric model generator ModGen. The core of the modeling concept consists of forming the basic load carrying sub-components such as spars, ribs and the skin. Therein the geometric library DT_NURBS [12] provides the means to describe these parts by Non-Uniform Rational B-Splines (NURBS). A variety of different methods is available to perform basic geometric operations such as the calculation of intersections of parametric curves with surfaces or the interpolation of geometric points. These mathematical descriptions and operations are the basis for the derivation of the finite element models of each component. The lifting surfaces' skins, ribs and spar webs are modeled as shell elements, while stringers, spar caps and other stiffeners are represented by beam elements. The

fuselage is modeled with beam elements as well, using two-dimensional tube-like cross sections. All the basic material and additional geometric properties of the elements are derived in the first level preliminary design stage and are available to the main loads process from the start. Together with parameterized interface models (e.g. connections between wing and fuselage, or pylon and wing) a structural model of a complete aircraft is assembled.
In order to reduce computation times, the full FEM model is reduced employing the static residualization approach proposed by Guyan [13] and available in NASTRAN. This method produces a matrix that condensates the components' stiffness properties onto a select number of degrees of freedom forming the so called loads reference axis (LRA). Usually these DoF lie close to the elastic axis, are not part of the FEM structure and hence do not have stiffness coefficients assigned to them. In order to obtain a physically reasonable reduced stiffness matrix that appropriately represents the elastic properties of the full FEM model, the LRA grid points are attached to the stiffest grid points of the FEM. Figure 3 shows this for a sub-section of the wing box. Here RBE3 elements are used, whose least-squares approach leads to a less harsh and more realistic connection compared to using rigid constraint equations. This not only results in a noise-free stiffness distribution, but a cleaner full model response when re-introducing LRA loads as well. The disadvantage of the LRA DoF becoming dependent can be overturned via the RBE3's UM-option that inverts arbitrary dependencies as long as rigid body motion is conserved.
The reduced model of the XRF1 consists of less than 3000 DoF compared to the full model's 72000 DoF. Because of its field of application it is often referred to as the 'dynamic master model' (DMM).

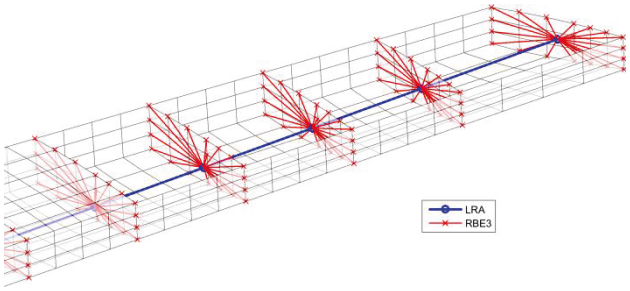

Figure 3. RBE3 spiders connecting the condensed and full model DoF.

Certain solution types, such as NASTRAN's flutter module or the transient simulation of integrated models, are based on systems with generalized states. The modal basis of flexible mode shapes and corresponding frequencies necessary to feed the linear flexible equations of motion were calculated from linear modal analysis. Higher frequency modes, which are less relevant to the global flexible behavior, are then eliminated from the resulting modal basis. This further reduces the number of DoF to 40 in case of the XRF1 and consequently speeds up calculation times even more.

3.2. Mass Model

The mass cases relevant for the loads calculation process are assembled by the preliminary sizing module. Generally this encompasses the secondary, fuel and structural masses. Secondary masses such as power units, systems, furnishing, operational items, passenger and payload masses are given by other pre-design tools. For example the detailed fuselage mass model is calculated by the fuselage cabin design tool FUCD developed by DLR [9].
The point masses are then written to the CPACS data file that is exchanged in the MDO process. Fuel masses are not provided by the dataset, but calculated from integrating the defined tank volumes considering a variety of different fill levels. Both the lumped secondary and fuel masses are attached to the nearest neighbor condensation point so that the number of DoF does not change (see Figure 4). The structural masses are naturally integrated by the FEM solver onto the full model's nodes and subsequently statically residualized using the same Guyan transformation applied to the stiffness matrix. These mass matrices can then be added to form a single mass case. In order to establish those mass cases most vital for critical loads, multiple payload and fuel combinations are considered and analyzed. Their importance is not only measured by the amount of mass, but the distance of their centers of gravity (CoG) to the aerodynamic center accounting for effects due to rotatory rigid body motion as well. At least the most forward and aft CoG positions for the most light and heavyweight designs have to be examined. For the XRF1 five mass cases are able to cover the weight and balance envelope. They are shown in Figure **5**, where the CoG offset from the leading edge is normalized with the Mean Aerodynamic Chord (MAC) and given in percent.

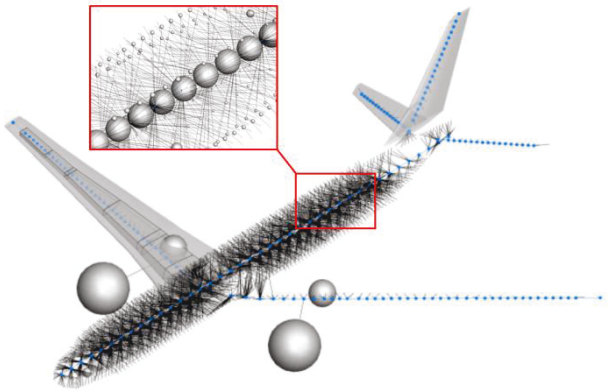

Figure 4. Secondary and primary lumped masses of the condensed structural grid.

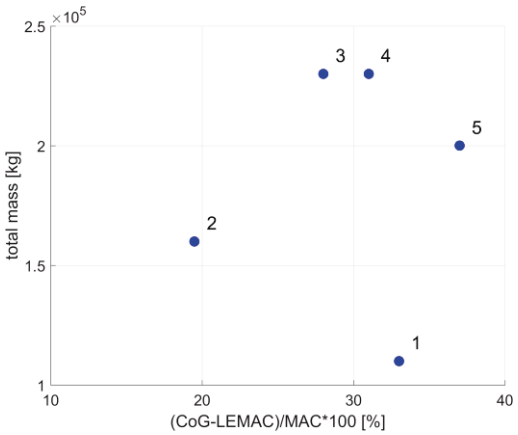

Figure 5. Weight and balance diagram.

3.3. Aerodynamic Model

One of the key aspects in model generation is the calculation of aerodynamic forces, where the right balance between accuracy and calculation time has to be found. Because many thousands of cases are usually considered in the loads calculation process, lower order, potential theory methods are used rather than high-fidelity computational fluid dynamic (CFD) solvers to determine aerodynamic coefficients. The governing equations of full potential theory can be derived from the Navier-Stokes equations of mass conservation, momentum and energy laws under the assumption of inviscid flow and an irrotational and isentropic flow field. Further linearizing the full potential theory equations leads to the Prandtl-Glauert equations,

$$\left(1-Ma^2\right)\frac{\partial^2\phi}{\partial x^2}+\frac{\partial^2\phi}{\partial y^2}+\frac{\partial^2\phi}{\partial z^2}-\left(\frac{2U}{a^2}\right)\frac{\partial^2\phi}{\partial x\partial t}-\left(\frac{1}{a^2}\right)\frac{\partial^2\phi}{\partial t^2}=0$$

The vortex lattice method (VLM) [14] solves the steady Prandtl-Glauert (Laplace) equation, where all lifting surfaces are discretized into boxes such as the one depicted in the red box in Figure 6. The three vortex lines are horse-shoe shaped and form a unique potential solution given a specific velocity that specifies the non-permeability boundary condition at the 3/4-chord control point normal to the box. The Kutta-Joukowsky theorem then allows to calculate the pressure difference between upper and lower sides of the box. Solving the problem for a whole discretized mesh with interactions between all boxes, then leads to the so called aerodynamic influence coefficient (AIC) matrix, which relates the differential box pressures to the boundary normal velocities. While the VLM is used to calculate the steady pressure contributions, the doublet lattice method (DLM) [15] is used to determine the unsteady, reduced frequency dependent incremental pressures which are especially important in gust calculations and necessary for determining flutter instabilities. It uses the same discretization as the VLM, but with a doublet potential distribution along the 1/4-chord line to solve the unsteady Prandtl-Glauert equation directly. By using the acceleration potential instead of the velocity potential, the differential pressures become available without the requirement for wake modeling. The resulting incremental complex valued coefficient matrices are then augmented by the steady vortex lattice AICs at all reduced frequencies.

The unsteady DLM aerodynamic model is only available in frequency domain and thus cannot be used in the time domain simulations of the maneuver loads tool without further processing steps. Roger's Rational Function Approximation [16] is therefore employed for the transient simulations, which allows for a conversion to time domain by a simple Laplace back-transformation. The approximation equation for the aerodynamic forces depends on the Laplace variable $\boldsymbol{s}$ and can be cast as (see [17]),

$$\boldsymbol{Q}(\boldsymbol{s})=\boldsymbol{A_0}+\boldsymbol{A_1 s}+\boldsymbol{A_2 s^2}+\boldsymbol{D}(\boldsymbol{sI}-\boldsymbol{R})^{-1}\boldsymbol{Es}$$

where $\boldsymbol{Q}$ are the total aerodynamic forces, $\boldsymbol{A_0}$ are the steady forces and $\boldsymbol{A_1}$ and $\boldsymbol{A_2}$ are the equivalent aerodynamic damping and mass matrix. The last term including a user given set of approximation poles $\boldsymbol{R}$, describes the lagging behavior of the forces and thus captures the phase shift of the complex frequency domain forces. Apart from a set of different approximation options such as weighting and the choice of poles, the accompanying matrices to the equation only depend on the discrete source AICs. The approximated forces have to be generalized by rigid body, flexible and control surface modes to be used in conjunctions with the generalized equations of motion.

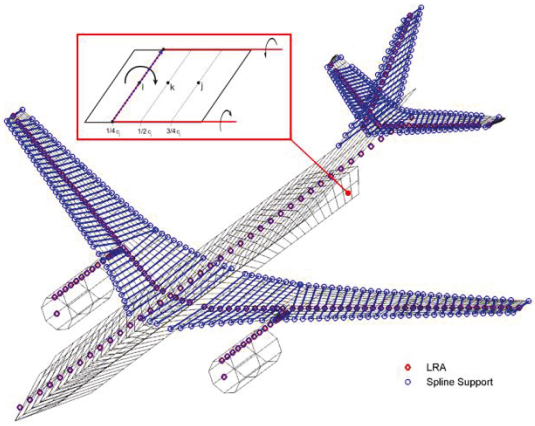

Figure 6. VLM/DLM panel mesh, LRA (red diamonds) and the spline support grid (blue circles) of the XRF1.

The panel models are derived from the CPACS aircraft geometry by ModGen including all lifting surfaces as well as engines and pylons. To account for lateral fuselage loads and for a better approximation of the aerodynamic effects between fuselage and lifting surfaces, the fuselage has an

additional perpendicular vertical plane. Control surfaces are established simply by combining panels and associate them with the specific hinge line information, such that the panel motion and the resulting panel downwash due to a deflection can be calculated. Camber and twist effects are calculated from geometrically-derived, local angle of attack information and are currently only regarded as additional constant downwash on the panels.

3.4. Model Integration

By combining a traditional linear and nonlinear rigid body flight dynamics model with linear aeroelastic dynamics, the equations of motion of the flexible aircraft can be derived. These equations combine the rigid body motion of the aircraft and the elastic deflections with respect to a body fixed system. Details may be found, for example, in Buttrill et al. [18], Waszak and Schmidt [19] and Waszak and Buttrill [20]. After a couple of simplifying assumptions and constraints, the nonlinear rigid body and flexible equations can be decoupled and are then available in their traditional form. The flexible part of the integrated model considers the representation of the aircraft by a chosen number of linear elastic modes obtained through a linear normal modes analysis of the structural model using the updated mass and stiffness matrices and optionally a modal damping matrix. Rigid motion is defined by six rigid body modes corresponding to the six degrees of freedom of a body reference frame fixed to the center of gravity in three-dimensional space. The classic linear elastic equations of motion are then generalized by the elastic modes and driven by the corresponding generalized coordinates. All external forces have to be generalized with the rigid and flexible modes of the structure to be compatible with the equations of motion. Doing so couples the flexible to the rigid equations of motion using the generalized AICs excited by either rigid body, flexible or control surface motion. In case other external forces are not defined in body axes, they have to be transformed beforehand as done with the gravity forces in inertial coordinates.

These equations and assumptions are, with some variation, the basis for both the MONA trim loads and the Varloads maneuver loads module. In the MONA module, NASTRAN employs the linearized Newton-Euler equations in frequency domain to solve the flexible trim and other aeroelastic problems. Varloads retains nonlinear rigid body motion in its time domain models to allow for control design by capturing the effects of rapid maneuvers more accurately [21].

4. LOAD CASES

4.1. Load Case Description

The load factors and design speeds to establish the flight envelope (see Figure 7) for loads estimation are calculated in accordance with the FAR §25.335 and §25.337 requirements [10]. The design cruise speed (V_C/M_C) is set to be equal to the maximum operating speed (V_{MO}/M_O) and taken as input, coming from the aircraft requirements. Compressibility effects are taken into account to define the stall speed V_S and manoeuver speed V_A by providing the aerodynamic derivatives $C_{A,max}(Ma)$, $C_{A,min}(Ma)$ and $C_{A,\alpha}(Ma)$. These values for the considered configuration were calculated by CFD analysis using the DLR code TAU [22] and provided through CPACS by project partners. The outputs are the structural design speeds for several altitudes and mass models as well as the corresponding maximum and minimum vertical load factors.
From this database the trim cases are defined to be calculated in the aerodynamic-structural coupled flight loads calculations. The flight loads trim definitions include symmetric, yawing and roll manoeuver flight conditions. The symmetric maneuver specifications (FAR §25.331) encompass trimmed aircraft conditions for pull-up and dive maneuvers with zero pitching acceleration. The yawing load cases are treated as a series of step inputs of the pilot that lead up to the four characteristic flight states explained in FAR §25.351. This includes two rapid acceleration cases, one quasi-steady case and a maximum sideslip angle case, as further explained in the next section. The rolling conditions are defined as a step input to the lateral stick controls (FAR §25.349). The analysis includes a pull-up roll with two-thirds of the maneuvering load factor and a dive roll with a load factor of zero. In each of the two cases the roll onset of sudden aileron deflection to the stop and the roll equilibrium of constant steady roll rate are examined.

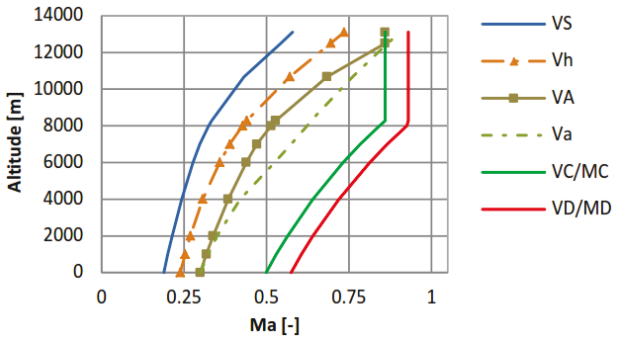

Figure 7. Flight envelope of the XRF1 aircraft.

The gust encounters are carried out in a series of transient simulations performed by the maneuver loads module. The rational function approximation

outlined in section 3.3 is employed to obtain a time-domain formulation of the required unsteady aerodynamic forces. Currently only the discrete, 1-cosine gust excitation profiles described in FAR §25.341 are considered. They are calculated for 5 different gust gradients between 30 ft. and 350 ft. coming from 4 directions. All these flight load cases are applicable to different sets of design speeds and a variety of altitudes and mass cases. For all the Digital-X XRF1 application examples this results in 1497 trim load cases each to be considered during the loads process.

4.2. Load Recovery and Loads Envelope

Two different methods exist to recover the forces and moments on the LRA degrees of freedom that form the balanced equilibrium stress state during flight of an aircraft model with a generalized description of flexibility. The less common but very simple recovery method is the so called Modal Displacement Method (MDM), where the internal nodal forces are derived from flexible deformation using the stiffness matrix. The disadvantage of this method lies within the fact, that the transient solutions are based on generalized coordinates, leading to a loss of information that depends on the number of flexible modes retained in the integrated model. Therefore the maneuver tool uses the Force Summation Method (FSM). This method recovers not the internal, but the external forces acting on the structure and thereby avoids the use of the integrated generalized flexible coordinates and the problematic generalization of some of the concentrated external loads such as engine thrust. This measurably improves the quality of the recovered loads (e.g. [11], [23]). The trim solutions performed by NASTRAN are not based on a generalized description of flexibility using free-free normal modes of the structure, but remain in the residualized DoF set. The problem of obtaining the deformation of the aircraft in free flight is instead solved by the inertia relief approach proposed by Rodden [24] and the recovery is performed by calculating the internal forces using the stiffness matrix and the non-generalized flexible states.
To establish a smaller series of critical loads that can be utilized by structural departments to formulate the boundary conditions for detailed structural analyses, the large amount of calculated loads is reduced by a loads selection scheme. The nodal loads are first integrated along the LRA-tree towards the root with respect to a set of automatically determined cut coordinate systems and corresponding structural grid point allocations. These cut loads are then used as the criteria to find a combination of cases that leads to the most extreme structurally stressed state. In one-dimensional envelopes this means determining the load cases with the largest and lowest cut forces and moments for each degree of freedom at each cut station. In two-dimensional envelopes those cases forming a convex-hull around correlated loads, e.g. the bending and torsional moments in a transient dynamic gust series, are picked. This allows to determine and analyze the driving cases of a design, reduces calculation time of subsequent design processes and raises efficiency of the structural optimization in the loads process itself.

5. TRIM CASE VERIFICATION

The FAR-based load conditions outlined in the previous section are solved by NASTRAN using the linearized rigid body equations of motion coupled aerodynamically to the linear elastic description for structural deformation in state-space form. Instead of examining the transient response, steady-state solutions of the frequency-domain system of equations are sought that must be able to cover the whole spectrum of internal forces and moments in terms of criticality. In order to determine the case-appropriate boundary conditions and to verify if those load conditions specified by the certification rules are sufficient, the yaw and roll maneuvers were subjected to transient, closed-loop maneuver simulation and analysis.

5.1. The Yaw Maneuver

According to FAR §25.351 the general yaw maneuver can be described by four consecutive characteristic states:

1. “Onset”: Starting from a level flight trim condition with zero sideslip, the rudder is rapidly deflected to the stop.
2. “Overswing”: As a reaction to the sudden deflection, a sideslip overswing behavior occurs that leads to a maximum sideslip angle.
3. “Equilibrium Yaw”: The rudder deflections are kept constant until a steady state with constant sideslip is reached.
4. “Rudder Return”: Out of the steady state, the rudder rapidly moves into its original trim position.

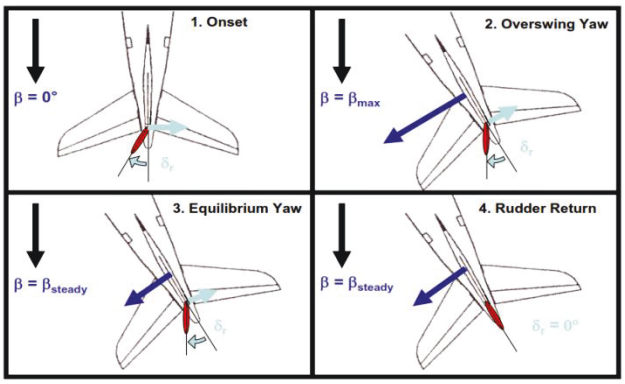

Figure 8. Characteristic states of the yaw maneuver.

A cascade controller [25] was used to maintain altitude while transmitting a pilot yaw command with different degrees of yaw damping to the actuation system. The yaw damper subtracts the measured yaw rate from the yaw rate commanded by the pilot to obtain the current rate error. This error multiplied by the damping strength k_r is fed back as a direct rudder deflection input. The low-frequency content of the steady yaw rate contribution in the measured signal is dropped by employing a high pass filter. The rudder deflection is restricted by a Rudder Travel Limitation Unit (RTLU) to avoid dangerously high loads. In order to assess the four trim cases displayed in Figure 8 they are now compared to the equivalent closed-loop dynamic simulation response for zero and high strengths of damping k_r. As the criterion to measure the effects on loads, the flap-wise bending moment Mx and the torsional moment Mz of the vertical tail plane were chosen. The results in terms of correlated Mx/Mz loads are displayed in Figure 9. As one can see the onset, equilibrium yaw and rudder return states obtained by the trim calculations (black) form the outer most critical points of the highly damped loads response (blue). The enveloping curve of the trim solutions thus covers that of the closed-loop system and therefore the critical trim loads are able to approximate those actually experienced in physical flight. The picture is different for the undamped case, where the overswing in loads is clearly visible, spiraling about the Equilibrium Yaw point. This poses a problem, because there is not a single overswing trim case that is able to generate a convex-hull that covers all critical overswing loads. Neither are the authors currently aware of a fast and reliable way to accurately predict a set of overswing points through trim calculations that accomplishes that task, especially not in the presence of an electronic flight control system. The conclusion drawn from this study is that in order to capture the overswing loads, closed-loop transient yaw maneuver simulations have to be performed for all design speeds between V_{MC} and V_D in the future.

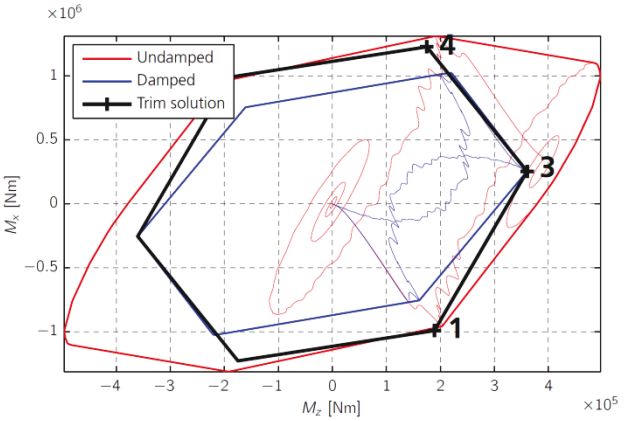

Figure 9. Correlated load and trim envelopes for a yaw maneuver.

5.2. The Roll Maneuver

Similarly to the yaw maneuver, the roll maneuver trim cases were verified as well. Following FAR §25.349 the general roll maneuver can be described by 3 consecutive characteristic states:

1. “Onset“: Starting from a pull-up or dive trim condition the ailerons are rapidly deflected to the stop.
2. “Equilibrium Roll”: The aileron deflections are kept constant until a steady state with constant roll rate is reached.
3. “Aileron Return”: Out of the equilibrium state, the ailerons are rapidly deflected in the opposite direction by half the angle of the onset.

The same cascade controller as in the yaw maneuver case was used to maintain the prescribed load factors of zero and two-third of the limit load at the equivalent airspeed in question. Figure 10 shows the roll maneuver response in form of the right wing bending moment M_y and torsional moment M_x correlated time track at a cut station close to the inboard edge of the ailerons. The transient dynamic response of the right roll maneuver is depicted by the thin red line and the left roll is depicted by the thin blue line. The thick red line forms the convex-hull for both cases combined. The results of the three trim cases and their convex-hull are displayed again in black. As can be seen, the equilibrium point of constant roll rate is captured very well, whereas both the accelerated roll cases’ maximum loads cannot be replicated exactly. This is in part due to the effects of large flexible overswing in bending and torsion similar to the sideslip overswing in the yaw case. Furthermore the electronic flight control system influences the flight state so that e.g. the desired load factor cannot be held constant exactly. Also there is a disparity between pilot command and physical aileron deflections which makes it difficult to predict accurate boundary conditions for the trim solution. A study to work out the major dependencies and rules of how to estimate roll and yaw maneuver boundary conditions in an efficient way is highly suggested. Until such a study has been conducted, the response of a transient dynamic roll maneuver is required as well to obtain the structural loading conditions of the open and closed-loop system.

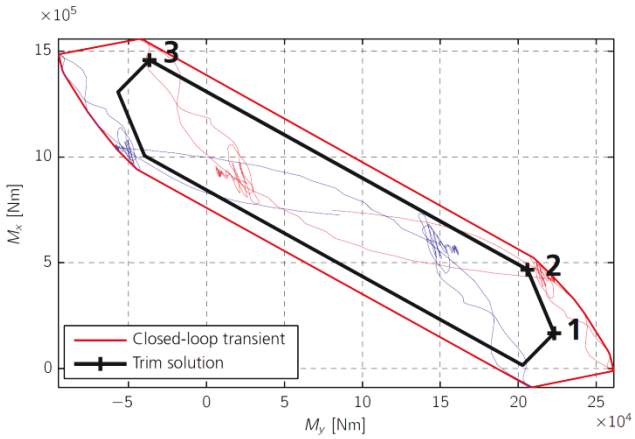

Figure 10. Correlated load and trim envelope for the roll maneuver.

6. AILERON REVERSAL CASE

Aileron reversal is the effect, where a flexible aircraft rolls in the opposite direction of the actual aileron input. This effect can occur if the wing structure has an insufficient torsional stiffness combined with flying near transonic speed at a high dynamic pressure. When e.g. the right aileron is deflected downward, an additional local lift is generated whose resultant introduces a bending moment about the elastic axis that twists the wing. This twisting leads to negative local angles of attack resulting in a down force that more than compensates the aileron input. Aileron reversal is a problem that has to be avoided, since a pilot that is not aware of the situation is likely to be confused, commanding roll inputs that lead to unintended, dangerous flight maneuvers.
A reference configuration of the XRF1´s control surfaces (Figure 11, left wing) has been prone to the aileron reversal effect.

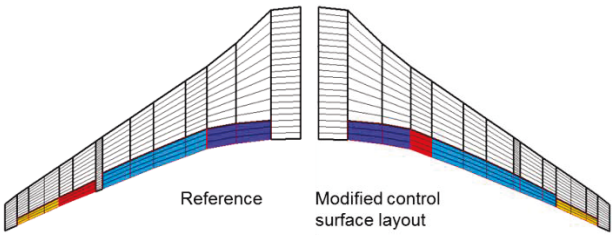

Figure 11. Aerodynamic panel model of the XRF1 wing with the original control surface placement on the left side and the modified placement on the right side. source: [1].

There are two ways to avoid the effect of aileron reversal. For one, the roll surfaces can be split in a high speed aileron that lies inboard of the wing (red surface on the right wing in Figure 11) and a low speed aileron outboard of the wing (yellow surface on the right wing in Figure 11). In this configuration solely the inner aileron is used to roll at high speed and the outer aileron solely at low speed flight. It has been shown, that the XRF1 configuration with a high speed aileron at the kink of the wing shows no aileron reversal behavior while achieving roll rates in all points of the flight envelope that satisfy the FAR requirements. If no high speed aileron is present, the torsional stiffness of the wing is increased by constraints imposed on the aileron efficiency of the aircraft that leads to a local thickening of the primary structural components like skin, spars and ribs. Such a constraint has been incorporated in the loads process of the Digital-X MDO framework using NASTRAN's SOL200 gradient-based optimizer with the objective to minimize the wing's structural weight. Figure 12 shows the XRF1's modified offset thickness distribution of the wing box after the sizing process. The initial wing had an overall thickness distribution determined by a sizing without aileron reversal constraints.

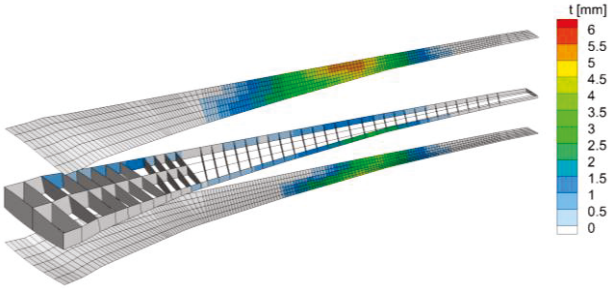

Figure 12. Change in the shell element's thickness distribution due to the sizing with aileron efficiency constraints, source: [1].

As can be seen, the primary structure has been strengthened in the middle part of the wing, gaining as much as six millimeters in thickness. This increases the torsional stiffness in the region right before the outer aileron and thus prevents overly large twisting of the outer wing due to an aileron deflection. The constraint is paid for by an increase in the primary wing structural mass of about five percent.

7. SUMMARY AND OUTLOOK

The automated MONA/Varloads main loads process within the Digital-X MDO framework has been outlined. This included structural, aerodynamic and mass model generation based on the parametric CPACS aircraft description. The basic methods for building the integrated flexible models for the trim and dynamic maneuver simulation modules have been explained along with the load recovery and selection schemes to determine the critical design loads. The approximate trim solutions for yaw and roll maneuvers have been compared to closed-loop maneuver transient response in order to assess their validity and uncover the scope of application. Furthermore the impact and necessity of including aeroelastic constraints in the sizing process have been demonstrated by incorporating aileron reversal constraints and showing their effect on the structural

dimensions of the wing box.
The goals of ongoing work in progress are mostly concerned with effects that are not yet captured by the integrated models. One example would be the integration of transonic effects by correcting the AIC-matrices with data interpolated from CFD-calculated pressure distributions [26]. Another important aspect is the inclusion of maneuver loads alleviation tables, which leads to quite a different magnitude and composition of the critical loads on the wing. Furthermore some important load conditions are not yet considered, such as the continuous gust or landing gear cases. Incorporating these missing pieces in the near future will lead to a loads process that is able to provide a full set of design loads that covers all major components of a transport type aircraft.

Bibliography

[1] R. Liepelt, V. Handojo, T. Klimmek, „Aeroelastic Analysis Modelling Process to Predict the Critical Loads in an MDO Environment," in *IFASD*, 2015.

[2] J. Hofstee, T. M. Kier, C. Cerulli, G. H. N. Looye, „A Variable, Fully Flexible Dynamic Response Tool for Special Investigations (VarLoads)," in *IFASD*, 2003.

[3] T. M. Kier, J. Hofstee, „Varloads - Eine Simulationsumgebung zur Lastenrechnung eines Voll Flexiblen, Freifliegenden Flugzeugs," in *DGLR*, 2004.

[4] T. Klimmek, „Parametrization of Topology and Geometry for the Multidisciplinary Optimization of Wing Structures," in *CEAS*, 2009.

[5] W. P. Rodden, E. H. Johnson, „MSC. Nastran Version 68 Aeroelastic Analysis User's Guide," 2004.

[6] S. Görtz, Č. Ilić, R. Liepelt, et al., „Collaborative Multi-level MDO Process Development and Application to Long-ranged Transport Aircraft," in *ICAS*, 2016.

[7] T. Zill, D. Böhnke, B. Nagel, „Preliminary Aircraft Design in a Collaborative Multidisciplinary Design Environment," in *AIAA ATIO*, 2011.

[8] D. Seider, S. Zur, J. Flink, R. Mischke, O. Seebach, „RCE - Distributed, Workflow-driven Integration Environment," in *EclipseCon Europe*, 2013.

[9] G. P. Chiozzotto, „CDloads: Conceptual design loads estimation.," *Tech. Rep.*, *DLR*, Göttingen 2013.

[10] F. A. Administration, *Federal Aviation Regulations Part 25 C, Airworthiness Standards: Transport Category Airplanes,* 2010.

[11] C. Reschke, „Flight Loads Analysis with Inertially Coupled Equations of Motion," in AIAA AFMC, 2005.

[12] B. Ames, „DT_NURBS Spline Geometry Subprogram Library, Theory Document, Version 3.6," 1998.

[13] R. J. Guyan, „Reduction of Stiffness and Mass Matrices," *AIAA Journal,* Bd. 3, p. 380, 1964.

[14] S. G. Hedman, „Vortex Lattice Method for Calculation of Quasi Steady State Loadings on Thin Elastic Wings, Technical Report 105," *Tech. Rep.*, *Aeronautical Research Institute of Sweden*, October 1965.

[15] E. Albano, W. P. Rodden, „A Doublet-Lattice Method for Calculating Lift Distributions on Oscillating Surfaces in Subsonic Flow," *AIAA Journal,* 1969.

[16] K. L. Roger, „Airplane Math Modeling Methods for Active Control Design," in *AGARD Structures and Materials Panel AGARD-CP-228*, April 1977.

[17] T. M. Kier, G. H. N. Looye, „Unifying Manoeuvre and Gust Loads Analysis Models," in *IFASD*, 2009.

[18] C. S. Buttrill, T. A. Zeiler, P. D. Arbuckle, „Nonlinear Simulation of a Flexible Aircraft in Maneuvering Flight," in *AIAA FSTC*, Monterey, 1987.

[19] M. R. Waszak, D. K. Schmidt, „Flight Dynamics of Aeroelastic Vehicles," *Journal of Aircraft,* June 1988.

[20] M. R. Waszak, C. S. Buttrill, „Modeling and Model Simplification of Aeroelastic Vehicles: An Overview," *Tech. Memo. 107691*, *NASA*, 1992.

[21] M. Leitner, A. Knoblach, T. Kier, C. Moreno, A. Kotikalpudi, H. Pfifer, G. Balas, „Flight Dynamics Modeling of a Body Freedom Flutter Vehicle for Multidisciplinary Analyses," in *AIAA MSTC*, 2015.

[22] D. Schwamborn, T. Gerhold, R. Heinrich, „The DLR TAU Code: Recent Applications in Research and Industry," in *ECCOMAS CDF*, 2006.

[23] M. Karpel, E. Presente, „Structural Dynamic Loads in Response to Impulsive Excitation," *Journal of Aircraft, Vol. 32,* pp. 853-861, 1995.

[24] W. P. Rodden, J. R. Love, „Equations of Motion of a Quasisteady Flight Vehicle Utilizing Restrained Static Aeroelastic Characteristics," *Journal of Aircraft,* Bd. Vol. 22, pp. 802-809, 1985.

[25] R. Brockhaus, W. Alles und R. Luckner, Flugregelung, Springer, 2011.

[26] M. J. Verveld, T. M. Kier, et al., „Reduced Order Models for Aerodynamic Applications, Loads and MDO," in *DLRK*, 2016.